Thermal Control Design for Enhancing Tolerance of Large-Aperture Reflective Camera "Sun Transit" on Geostationary Earth Orbit

*LIAN Xinhao**, *XIA Chenhui*, *GAO Chao*

Beijing Institute of Space Mechanics & Electricity, Beijing 100094, P. R. China

(Received 28 March 2025; revised 10 July 2025; accepted 1 August 2025)

Abstract: The large-aperture reflective cameras on the geostationary orbit are susceptible to significant temperature fluctuations due to the "Sun transit" effect. To address the shortcomings of existing thermal control measures using camera sunshades to suppress the "Sun transit" and the issue of excessively large solar avoidance angles determined solely by geometric relationships, a thermal control design method is proposed that involves adding multi-layer thermal protection at the secondary mirror position of the camera. The goal is to optimize the avoidance angle and enhance the camera's tolerance to "Sun transit". A heat balance and motion relationship between the avoidance angle and duration is established. Then, the minimum solar avoidance angle after adopting the multi-layer thermal protection design is calculated. This angle is compared with the one determined by geometric relationships, leading to the conclusion that this method can effectively enhance the camera's tolerance to "Sun transit". A heat dissipation scheme is proposed that involves a coupled north-south heat spreader design with low-temperature compensation for the internal heat source. The calculation results of the two avoidance angles are applied to the calculation of the heat dissipation area and low-temperature compensation power, achieving a closed-loop heat dissipation scheme. Puls, the superiority of the multi-layer thermal protection design method is demonstrated from the perspectives of heat dissipation area and low-temperature compensation power requirements. A comparative analysis of simulation analysis, thermal balance tests, and in-orbit temperature data further validates the effectiveness of this method.

Key words: geostationary earth orbit; Sun transit, solar avoidance; thermal control design; thermal protection

CLC number: V444.3 **Document code:** A **Article ID:** 1005-1120(2025)04-0452-12

0 Introduction

High-resolution imaging satellites operating in the geostationary earth orbit (GEO) have technical advantages such as wide field of view, high temporal resolution, and strong response capabilities. They are increasingly becoming a research hotspot for major national and international space agencies[1-3]. The camera, as the main payload of the satellite, is a particular focus of this research[4-6]. In China, the main representative is the "Gaofen-4" satellite launched in December 2015. The satellite is used for land resource surveys, crop assessment, disaster monitoring and evaluation, weather monitoring and forecasting, forestry surveys, earthquake monitoring, and emergency response, etc. The payloads on board are large-aperture, reflective, integrated high-resolution cameras covering visible and infrared wavelengths[7-8]. The United States began developing geostationary remote sensing systems as early as 1970, with the Geosynchronous Space Situational Awareness Program (GSSAP) constellation being a typical example. Completed at the end of 2016, the constellation carries optical payloads primarily used for surveillance and observation of GEO satellites. It can approach and fly in formation to ob-

*Corresponding author, E-mail address: 13699226843@139.com.

How to cite this article: LIAN Xinhao, XIA Chenhui, GAO Chao. Thermal control design for enhancing tolerance of large-aperture reflective camera "Sun transit" on geostationary earth orbit[J]. Transactions of Nanjing University of Aeronautics and Astronautics, 2025,42(4):452-463.

http://dx.doi.org/10.16356/j.1005-1120.2025.04.002

tain high-definition views of key targets and is the main system currently used by the US military for routine surveillance of high-orbit targets[9-10]. Other countries are also developing geostationary remote sensing satellites in parallel, such as Europe's Meteosat, Japan's JAM, Russia's GOMS, India's INSAT, and South Korea's COMS[11-13].

GEO orbital thermal flux is characterized by large variations and low frequency[14], especially the "Sun transit" phenomenon at the camera's light inlet. Without proper thermal control design, it can easily cause thermal cycling in the camera's optical system, greatly affecting the camera's high-quality imaging, and may even cause irreversible damage to the optical system. Many researchers have studied GEO orbital camera thermal control technology, characteristics of external thermal flux, and its simulation methods[15-18]. The widely adopted thermal control method is to apply certain thermal control measures to the camera's light shield to suppress the impact of "Sun transit" and achieve the goal of controlling the temperature of sensitive areas within the camera such as secondary mirror, primary mirror. After adopting this method, the temperature fluctuation of the camera's primary and secondary mirror positions within one orbital cycle is about 1—2 ℃, which meets the index requirements, but there is a certain gap compared to the actual performance of low-orbit cameras with temperature fluctuations within 0.3 ℃[19-20]. The reason is that the suppression effect on "Sun transit" is still insufficient. Since the impact of "Sun transit" is so significant and the effect of suppression methods is limited, naturally, solutions are proposed from the source of "Sun transit", which is the direction of solar light incidence. One of these methods is to use satellite attitude maneuvering as an external force to avoid solar light from shining on the camera's light inlet. Some researchers have proposed specific control algorithms for satellite attitude avoidance maneuvers[21-22]. The core idea of the control algorithm is to convert the constraints of camera usage, onboard power constraints, dynamic constraints, etc., into spatial geometric relationship constraints, and thus select the optimal avoidance angle. The constraint condition of camera usage, that is, the minimum avoidance angle of the camera, is determined by the design state of the camera. From the perspective of the difficulty of achieving satellite attitude avoidance, it is obviously better to have a smaller angle. This article attempts to start from the camera thermal control design method, striving to reduce the temperature fluctuation of sensitive positions of the camera and optimize the avoidance angle, enhancing the camera's tolerance to "Sun transit".

1 Camera Thermal Control Design

1.1 Difficulties in camera thermal control design

The GEO orbit large aperture reflective camera features high resolution and long operational life requirements, necessitating the stability and uniformity of the optical system's temperature throughout its entire lifecycle. Moreover, due to the camera's large size, high power dissipation, and harsh external thermal conditions, the thermal control design faces significant challenges. Specifically, these challenges the following are as follows.

(1) The GEO orbit period is long (24 h) with drastic changes in external thermal flux and the presence of "Solar transits".

As shown in Fig.1, the variation pattern of the external thermal flux in all directions within the orbital plane ($\pm X$ and $\pm Z$, in this coordinate system: X points the direction of the satellite's flight, and $+Z$ points toward the Earth's center, as shown in Fig.2) is such that for half the period. The thermal flux value is zero. And for the other half, it changes according to a sinusoidal function. The amplitude is the projection value of the solar constant S within the orbital plane (maximum around the equinoxes at approximately 1 360 W/m^2 and the minimum around the solstice at approximately 1 210 W/m^2). Each direction is 90° out of phase with the next, meaning that regardless of the camera's aperture orientation within any direction of the orbital plane, there is always solar radiation incident on the camera's optical system, i.e., a "Sun transit" situation.

The external thermal flux in the direction perpendicular to the orbital plane ($\pm Y$) is a stable

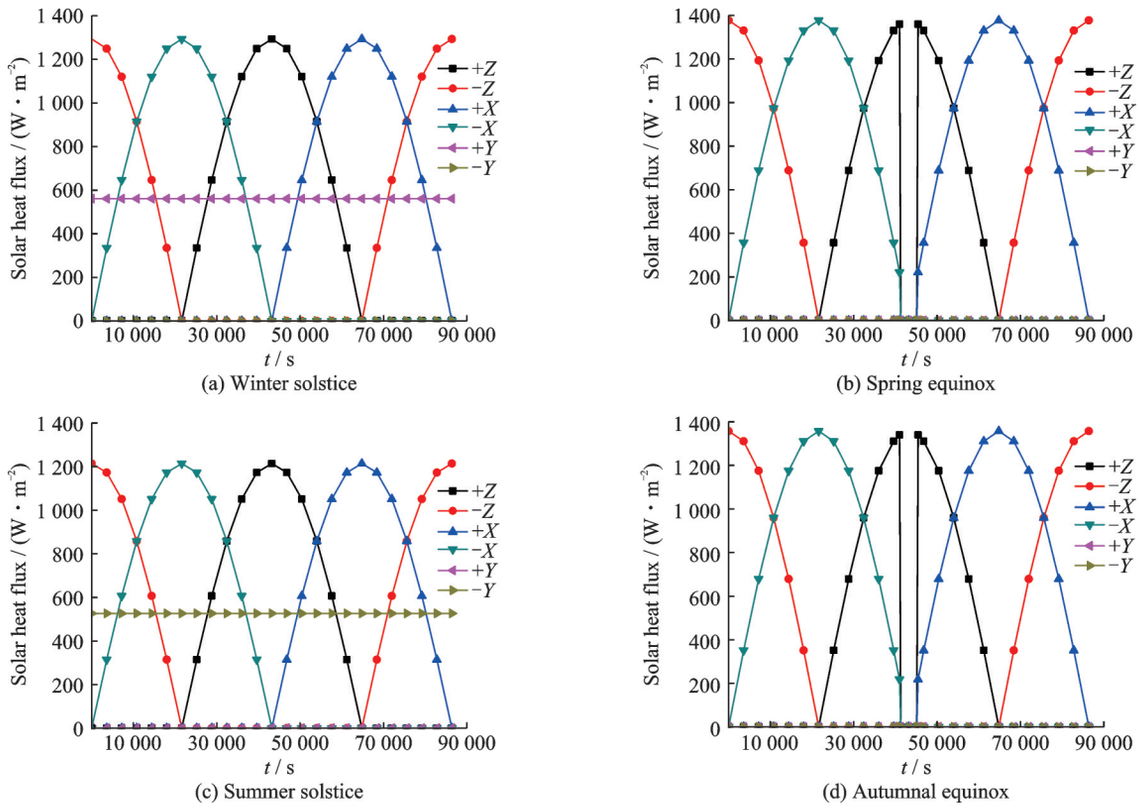

Fig.1 External thermal flux of GEO

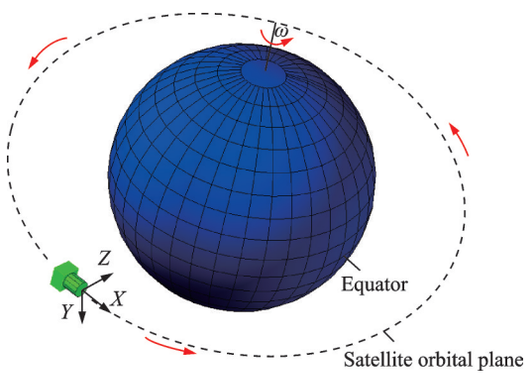

Fig.2 Definition of the satellite coordinate system

constant within the same orbital period and at any moment at least one direction has zero external thermal flux, making it a relatively ideal orientation for heat dissipation. However, its annual variation within the range of 0—560 W/m^2 poses considerable difficulties for heat dissipation design.

(2) A larger camera aperture means that the overall size of the camera will increase, which in turn leads to a larger satellite platform. This presents two challenges: Firstly, the distance for heat transfer from the camera heat source to the cooling surface becomes longer, which increases the difficulty of thermal design; Secondly, the satellite's moment of inertia increases, making it more difficult to control if satellite attitude maneuvers are used to avoid "Sun transit".

1.2 Thermal control design to enhance the camera's tolerance to solar transit

The basic idea of the thermal control design aiming at enhancing the camera's tolerance to "solar intrusion" is as follows. (1) Carry out structural temperature control design and a pre-liminary scheme for internal heat source dissipation; in the structural temperature control design, strengthen thermal protection at sensitive locations to reduce the impact of direct solar heat flow. (2) Calculate the heat flux that still reaches the camera's sensitive areas after thermal protection design and the resulting temperature fluctuations. The heat flux corresponding to temperature fluctuations that exceed the specified range is the heat that needs to be eliminated through satellite attitude avoidance. Based on this, calculate the minimum avoidance angle. (3) Calculate and adjust the heat dissipation area under this avoidance angle, then, close the loop on the internal heat source dissipation design scheme.

1.2.1 Structural temperature control design and preliminary scheme for internal heat source dissipation

As shown in Figs.3, 4, the structure of a large-aperture reflective camera consists of a primary mirror assembly, a secondary mirror assembly, a main bearing plate, a barrel, and a hood, etc. The secondary mirror and the front part of the barrel are close to the light inlet and are prone to "Sun transit" disturbances. Therefore, thermal protection must be a key focus in the camera's thermal design. Specific measures for structural temperature control are as follows.

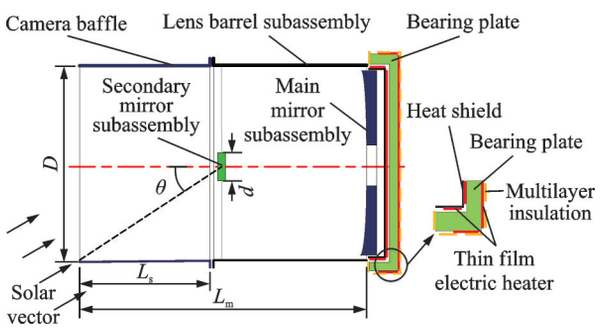

Fig.3 Camera optomechanical structure

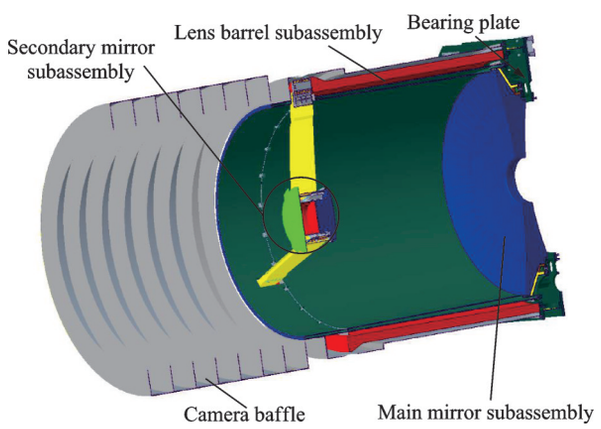

Fig.4 3D diagram of camera optomechanical structure

(1) A heat shield is designed on the back of the mirror (towards the lightinlet side), as shown in Fig.5. The groove space formed by the secondary mirrors-upport structure is utilized. The heat shield is designed in two parts, the inner and the outer. Each of them is covered with multiple layers of thermal insulation components, forming a double-layered structure to enhance the isolation effect against sunlight on the back of the secondary mirror. The outer surface of the secondary mirror frame is covered with multiple layers to prevent heat leakage to the outside. The installation positions of the secondary mirror frame, the secondary mirror internal heat shield, and the secondary mirror support structure adopt thermal insulation design. Heating circuits are placed at the positions of the secondary mirror internal heat shield and the secondary mirror frame to actively control the temperature of the secondary mirror.

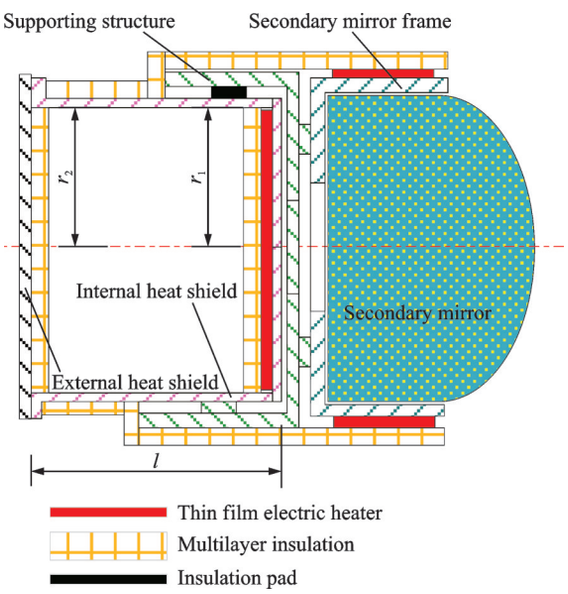

Fig.5 Thermal control method in secondary mirror subassembly

(2) The barrel, as the main structural component for carrying the secondary mirror assembly, any temperature-induced thermal deformation will directly affect the relative position of the primary and secondary mirrors, thereby affecting the imaging quality. Therefore, maintaining its temperature stability is crucial. The location of the barrel means that both its inner and outer walls can be exposed to sunlight. The focus of its thermal control design is to find a way to isolate the "doublesided attack" of sunlight. As shown in Fig.6, heat shields are added on both the inner and the outer sides of the barrel. The outer surface of the outer heat shield is covered with multiple layers of thermal insulation components to isolate sunlight, forming the first layer of thermal barrier. Multiple layers of thermal insulation components are covered on the outer surface of the barrel to form the second layer of thermal barrier.

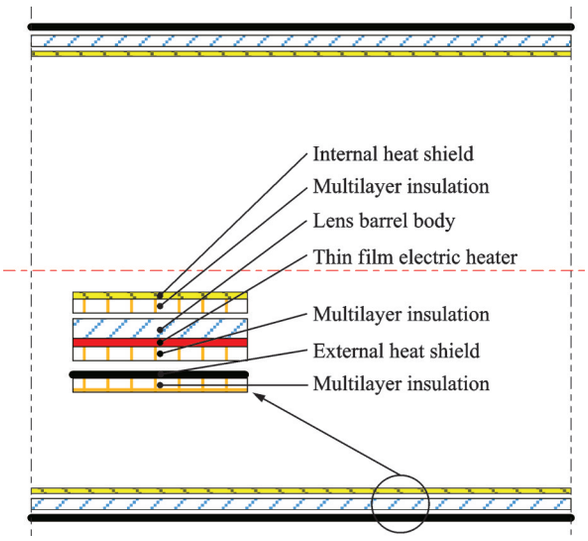

Fig.6 Thermal control method in lens barrel subassembly

Multiple layers of thermal insulation components are covered on the outer surface of the inner heat shield to form the third layer of thermal barrier. The first two layers of thermal barriers mainly isolate the heat flow on the outer wall of the barrel, while the third layer isolates the heat flow on the inner wall of the barrel. Heating circuits are arranged on the outer wall of the barrel for active temperature control.

(3) Heat shields are set up on the back and around the primary mirror, with heating circuits arranged on the heat shields to control the temperature of the primary mirror.

(4) Heating circuits are arranged on the main load-bearing plate to control its temperature, and the outer surface is covered with multiple layers of thermal insulation components to isolate heat transfer with the outside world.

Based on the characteristics of the external heat flow distribution, the internal heat source cooling adopts a north-south coupled cooling surface design. That is, the heat from the internal heat source is conducted to the nearest cooling surface through heat pipes, and the two cooling surfaces are connected by heat pipes to distribute the heat evenly, as shown in Fig.7. To maintain the stability of the cooling system and prevent the temperature from dropping too low when the internal heat source is not working, a heating loop is arranged at the position of the internal heat source for low-temperature compensation temperature control. The areas of the north and the south cooling surfaces are the same, and the radiation surfaces are all coated with optical sdar reflector (OSR) thermal control coating.

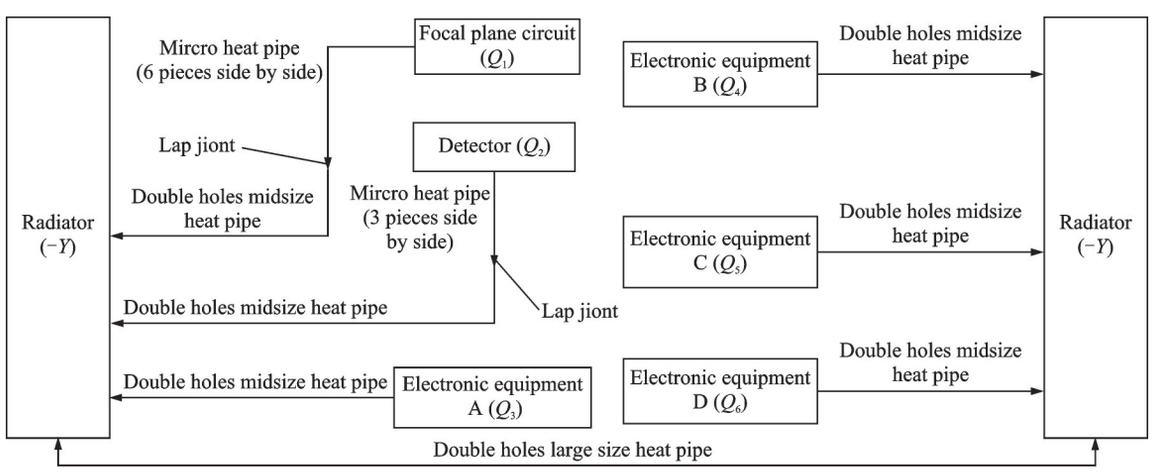

Fig.7 Heat dissipation paths of the internal heat source

A preliminary calculation is conducted for the heat dissipation area and low-temperature compensation power, assuming that the temperature control target for each internal heat source is $[T_{c,i}, T_{h,i}]$, the heat generated during operation is Q_i, and the thermal resistance from the internal heat source to the heat dissipation surface is R_i. Then the area A of the heat dissipation surface satisfies the following heat balance relationship

$$\sum_{i=1}^{n} Q_i + \alpha_{sh} A q_{s,max} = 2\varepsilon\sigma A \overline{T}_h^4 \qquad (1)$$

where α_{sh} is the maximum value of the solar absorption ratio of the heat dissipation surface thermal control coating, according to Ref.[10], and set as 0.24;

ε the thermal radiation rate, taken as 0.78; $q_{s,max}$ the maximum value of the solar direct heat flux reaching the heat dissipation surface, according to section 1.1, and set as 560 W/m^2; σ the Stefan-Boltzmann constant, with a value of 5.67×10^{-8} W/(m^{2}K^4); and $\overline{T}_h$ the temperature of the heat dissipation surface, which is taken as the average value of $\overline{T}_h = T_{h,i} - Q_i R_i$. By simple transformation of Eq.(1), the heat dissipation surface area A can be preliminarily calculated. The low-temperature compensation power is the minimum power required to maintain the lower limit of the internal heat source temperature control target under the conditions of the heat dissipation surface area being A, the internal heat source not working, and the minimum external heat flux as 0 W/m^2. P_i satisfies the energy balance relationship while being constrained by the thermal resistance R from the internal heat source to the heat dissipation surface, that is, it satisfies Eqs.(2, 3). Solving the Eqs.(2, 3) by iteration gives P_i and $\overline{T}_c$. $\overline{T}_c$ is the temperature of the heat dissipation surface, which is different from the temperature T in Eq.(1).

$$\sum_{i=1}^{n} P_i = 2\varepsilon\sigma A\,\overline{T}_c^4 \tag{2}$$

$$P_i = \frac{T_{c,i} - \overline{T}_c}{R_i} \tag{3}$$

1.2.2 Calculation of the minimum avoidance angle

As shown in Fig.3, the camera's light aperture diameter is D; the secondary mirror diameter is d; and the distance from the secondary mirror to the front end of the camera's light shield is L_s. If the angle θ between the solar light and the camera's optical axis is maintained $\theta \geqslant \arctan\dfrac{D+d}{2L_s}$, under the shielding of the camera's baffle, the solar light will not illuminate the secondary mirror assembly, so solar avoidance is not required. As the rotation of the satellite around the Earth, the angle θ gradually decreases, and the solar light will illuminate the back of the secondary mirror, causing a temperature rise in the secondary mirror, which requires avoidance. After adopting the thermal control measures described in section 1.2.1 for the secondary mirror position, the solar avoidance angle can be reduced. Assuming the minimum avoidance angle for solar light is θ_{min}, and the temperature rise ΔT of the secondary mirror does not exceed 0.3 K under the requirement, the required avoidance duration τ must satisfy the following heat balance relationship and motion relationship

$$c_m \Delta T = \varepsilon_1\varepsilon_2 X_{1,2} S \frac{\pi}{4} d^2 \cos\theta_{min}\cdot\tau \tag{4}$$

$$\theta_{min} = \frac{1}{2}\omega\tau \tag{5}$$

where c_m represents the thermal capacity of the secondary mirror, measured in J/K. ε_1 and ε_2 are the equivalent emissivities of the two layers of the multilayer insulation components of the secondary mirror[23], which are taken as 0.03 according to Ref.[24]. $X_{1,2}$ is the view factor from the external heat shield to the internal heat shield of the secondary mirror, and its calculation method is derived from Ref.[25]. $X_{1,2} = \dfrac{1}{2}\left[\kappa - \sqrt{\kappa^2 - 4\left(\dfrac{r_2}{r_1}\right)^2}\right]$, $\kappa = 1 + \dfrac{1+R_2^2}{R_1^2}$, $R_1 = r_1/l$, $R_2 = r_2/l$. And in practice, since the differences between r_1 and r_2 are small, R_1 and R_2 can be approximated as $R_1 = R_2 \approx d/21$, with l being the distance between the two disks. ω is the angular velocity of the satellite rotating around the Earth, with a value of $\dfrac{2\pi}{24}\times\dfrac{1}{3\,600} \approx 7.27\times10^{-5}$ rad/s. By combining Eqs.(4) and (5) and solving iteratively, θ_{min} and τ can be determined.

Taking a camera as an example with we have a clear aperture diameter D =610 mm, a secondary mirror diameter d=150 mm, a distance from the secondary mirror to the front end of the camera's light shield L_s =360 mm, a thermal capacity of the secondary mirror c_m=578 J/K, and a distance of l = 90 mm. Using the calculation formulas for κ and $X_{1,2}$, we find κ=2.36, $X_{1,2}$=0.55. Evidently, Eqs.(4, 5) cannot be directly solved analytically. Therefore, an iterative method is used to obtain their numerical solution, with angular calculation accuracy of 0.05°, and the initial angle value is set to θ_1=45°. By substituting θ_1=45° into Eqs.(4, 5), we obtain θ_{1c}=41.70° and τ_1 =20 024 s. Let θ_2 =

$0.5(\theta_1+\theta_{1c})=43.35^\circ$. Substitute this value back into Eqs.(4, 5) to calculate and obtain $\theta_{2c}=40.6^\circ$ and $\tau_2=19\ 472$ s. This process is repeated until the desired condition $|\theta_i-\theta_{ic}|<0.05^\circ$ is met. The specific calculation process is detailed in Table 1.The final results are $\theta_{min}=36.8^\circ$ and $\tau=17\ 683$ s.

Table 1 Calculation process of θ_{min} and τ

i	$\theta_i/(^\circ)$	$\theta_{ic}/(^\circ)$	τ_1 /s	$\lvert\theta_i-\theta_{ic}\rvert/(^\circ)$
1	45.00	41.70	20 024	3.30
2	43.35	40.55	19 472	2.80
3	41.95	39.65	19 023	2.30
4	40.80	38.96	18 705	1.84
⋮	⋮	⋮	⋮	⋮
16	36.79	36.81	17 863	0.02

It is important to further verify, by maintaining this avoidance angle, whether sunlight will be reflected onto the main mirror or not. The specific method is to determine whether $\theta_{min}\geqslant\arctan\dfrac{D}{L_m}$ can be established. The distance from the primary mirror to the front end of the light shield of the camera is $L_m=920$ mm, and since $\arctan\dfrac{D}{L_m}=33.5^\circ$, $\theta_{min}=36.8^\circ$ is greater than this angle, maintaining the solar avoidance angle ensures that sunlight will not be reflected onto the main mirror.

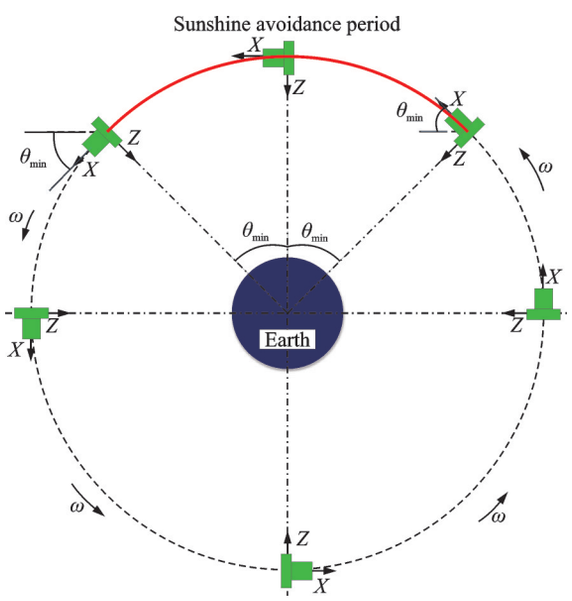

Fig.8 Diagrammatic sketch of avoidance angle and period

Compared to the avoidance angle $\theta=\arctan\dfrac{D+d}{2L_s}=46.5^\circ$ derived from geometric relationships, this avoidance angle has been reduced by 9.7°, indicating that after adopting thermal protection measures, the minimum solar avoidance angle has been decreased, enhancing the camera's ability to "Sun transit".

1.2.3 Closed-loop design for heat dissipation of internal heat sources

In the heat dissipation scheme for internal heat sources within section 1.2.1, the calculation of the heat dissipation surface area and the low-temperature compensation power did not consider the change in the angle between the solar rays and the heat dissipation surface caused by solar avoidance, which could lead to changes in the external heat flow of the heat dissipation surface, thereby adjusting the surface area and low-temperature compensation power. The attitude maneuvering methods that can be used for solar avoidance include rotation around the X-axis, which is rolling, rotation around the Y-axis, which is pitching, and rotation around the Z-axis, which is yawing. Taking the camera's optical port facing the X direction as an example, since the rolling method does not change the angle of solar incidence, solar avoidance cannot choose the rolling method. If pitching is chosen, because the heat dissipation surface is selected in the $+Y$ direction, the pitching avoidance method will not cause a change in the angle between the heat dissipation surface and the solar rays, and the heat dissipation surface area and low-temperature compensation power calculated using the method of section 1.2.1 will not change. Using the yaw method to avoid solar rays will cause the angle between the solar rays and the heat dissipation surface to increase, leading to adjustments in the heat dissipation surface area and low-temperature compensation power. The camera's optical port facing the Z direction is similar. Using the rolling method to avoid solar rays will cause adjustments in the heat dissipation surface area and low-temperature compensation power. The avoidance angles calculated in section 1.2.2, $\theta_{min}=36.8^\circ$, and the avoidance angles obtained from geometric relationships, $\theta=46.5^\circ$, are input into $q_{s,max}=S\sin\theta_{min}$ and $q_{s,max}=S\sin\theta$ to obtain new $q_{s,max}$. Using

these values to recalculate the heat dissipation surface area A and compensation power $\sum P_i$ according to Eqs.(1—3). The calculation results are compared with those in section 1.2.1, as shown in Table 2. The thermal resistance R_i from the internal heat source to the heat dissipation surface is not the focus of this paper and is only given as an input condition for calculation.

From the calculation results, it can be seen that after adopting avoidance measures, the solar direct heat flux reaching the heat dissipation surface increases, leading to an increase in the area of the heat dissipation surface and the low-temperature compensation power. This is the cost of adopting avoidance measures to deal with "solar transit". Relatively speaking, the secondary mirror position has adopted thermal protection measures, and the avoidance angle obtained from the relative geometric relationship is smaller. The solar direct heat flux reaching the heat dissipation surface will decrease, and accordingly, the area of the heat dissipation surface and the low-temperature compensation power will both decrease by about 10%, indicating that the secondary mirror thermal protection measures help to optimize the avoidance strategy and enhance the tolerance to "solar transit".

Table 2 Calculation results of A and ΣP_i under different avoidance angles

Internal heat source	Input condition				Not avoiding		$\theta_{min}=36.8^\circ$		$\theta_{min}=46.5^\circ$	
	Q_i/W	$T_{c,i}$/K	$T_{h,i}$/K	R_i/(K·W^{-1})	$\sum P_i$/W	A/m^2	$\sum P_i$/W	A/m^2	$\sum P_i$/W	A/m^2
Focal plane circuit	14	279	293	0.4	69.8	0.14	81.2	0.16	90.6	0.18
Detector	5	279	293	0.8	69.8	0.14	81.2	0.16	90.6	0.18
Electronic equipment A	3	279	298	0.3	69.8	0.14	81.2	0.16	90.6	0.18
Electronic equipment B	15	279	298	0.3	69.8	0.14	81.2	0.16	90.6	0.18
Electronic equipment C	13	279	298	0.3	69.8	0.14	81.2	0.16	90.6	0.18
Electronic equipment D	12	279	298	0.3	69.8	0.14	81.2	0.16	90.6	0.18

2 Design Verification and On-Orbit Application

To verify the effectiveness of the aforementioned design, simulation analysis and thermal balance tests were conducted. A thermal model of the spacecraft system was established using Thermal Desktop software, and the geometric model was appropriately simplified according to the needs of thermal analysis, neglecting the effects of the camera's internal microstructures on heat conduction and radiation. Local structural features such as screws were simplified, as shown in Fig.9. The avoidance angle and avoidance time were set according to the calculation results of the minimum avoidance angle in section 1.2.2, and calculations for high and low temperature conditions were performed. For high-temperature conditions, the external heat flux is taken at the winter solstice, with the camera installation boundary temperature at 25 ℃. The radiation properties of the radiators and the multilayer insulation component surfaces were taken as the values at the end of the lifetime. For low-temperature conditions, the external heat flux was taken at the spring equinox, with the camera installation boundary temperature at −10 ℃. The radiation properties of the radiators and the multilayer insulation component surfaces were taken as the values at the beginning of the lifetime. The main thermal properties parameters in thermal analysis were selected based on Refs.[26-28], and specific details are listed in Tables 3, 4.The internal heat source operated continuously for eight hours, and the operating time was able to cover the

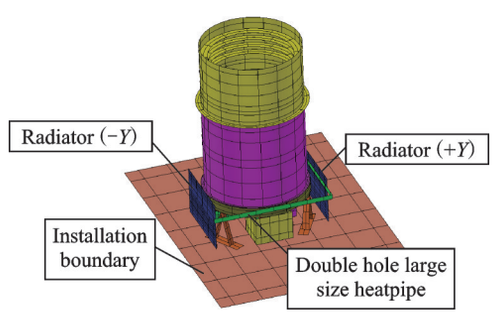

Fig.9 Thermal model of camera

avoidance period. The temperature variation curves of the primary mirror, the secondary mirror, and the detector over two orbital periods are shown in Fig.10.

Table 3 Key thermal properties in thermal analysis

Component	Material	Density/ ($kg \cdot m^{-3}$)	Thermal conductivity/ ($W \cdot (m \cdot K)^{-1}$)	Specific heat capacity/ ($kJ \cdot (kg \cdot K)^{-1}$)
Camera baffle	Carbon fiber	1 700	35	921
Main mirror	SiC	3 400	185	825
Secondary mirror	Glass-ceramic	2 530	1.64	821
Secondary mirror frame Bearing plate	TC4	4 500	8.8	678
Lens barrel body	C-SiC	2 000	20	700
Heat shield	Kevlar	1 440	0.04	1 420
Radiator	Aluminium alloy	2 700	130	921

Table 4 Radiation properties of radiators and the multilayer

Surface	Beginning/end of the lifetime	Solar absorption ratio α_s	Thermal radiation rate ε
Radiator	Beginning	0.12	0.78
	End	0.24	0.78
Multilayer	Beginning	0.36	0.70
	End	0.60	0.70

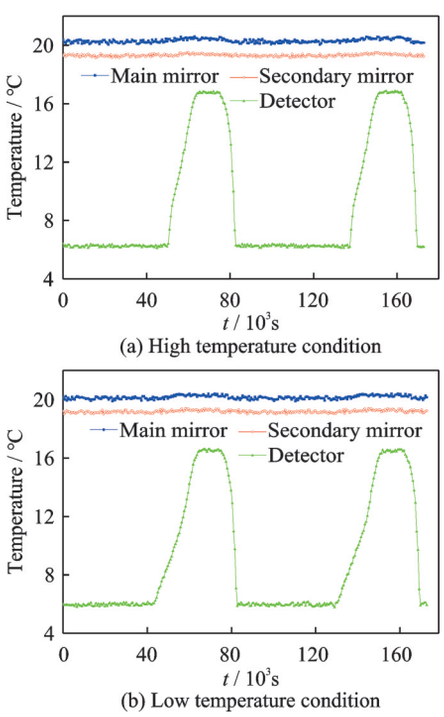

Fig.10 Temperature curves of thermal analysis

Thermal balance tests were conducted, with the thermal tests performed in a vacuum chamber. The inner wall temperature of the vacuum chamber was below 100 K. The vacuum degree was higher than 1.3×10^{-3} Pa, and the surface reflectivity is greater than 0.9. A thermal vacuum environment is effectively simulated. The test site is shown in Fig.11. During the tests, electric heaters were used to simulate the heat flow at the secondary mirror thermal shield and radiating surface positions. The position of the secondary mirror thermal shield was simulated by placing the electric heater on the outside of the outer thermal shield, and the heat flow at the heat dissipation surface was simulated by placing the electric heater on the radiating surface of the heat dissipation surface. The surface of the heat dissipation surface where the electric heater was placed was coated with a thermal control coating, with a surface emissivity of 0.78 ± 0.02, equivalent to the OSR radiation effect[29-30]. The heating power calculated according to the minimum avoidance angle in section 1.2.2 was loaded onto the simulated electric heater. The selection of the thermal balance test conditions completely corresponds to the thermal analysis conditions. The temperature variation curves of the primary mirror, the secondary mirror, and the detector within one orbital period are shown in Fig.12.

Comparing the thermal analysis calculations with the thermal balance test temperature data, we find the consistency is good. The temperature of the secondary mirror fluctuates around 19.2—19.4 ℃, and the temperature of the primary mirror fluctuates

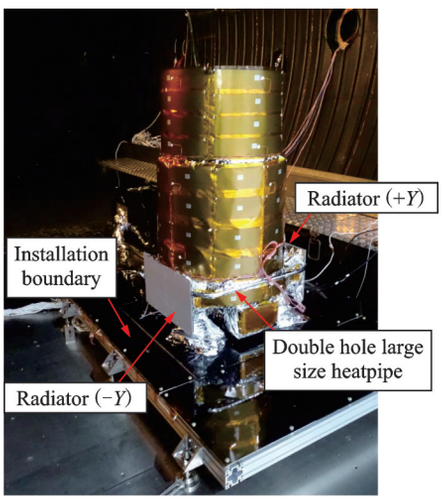

Fig.11 Picture of the camera thermal balance test in progress

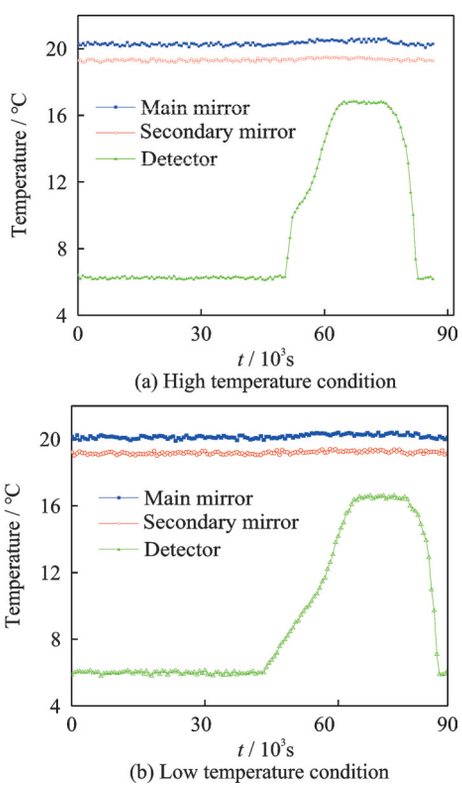

Fig.12 Temperature curves of thermal balance test

around 20.2—20.4 ℃. During the avoidance period, there is no significant temperature rise. The temperature of the detector is maintained around 5.9—16.2 ℃ during the eight hours when it is not working, and at that time, the temperature rises to a maximum of 16.8 ℃. It remains stable during the avoidance period, indicating that the thermal design method adopted is reasonable and effective. The proposed design method has been successfully applied to the Earth synchronous orbit satellite model launched at the end of 2021. After nearly three years of on-orbit operation, its camera thermal control system remains stable. In order to facilitate the comparison with simulation analysis and thermal balance test data, one year of on-orbit data for the primary mirror, the secondary mirror, and the detector positions was retrieved, as shown in Fig.13. The temperature of the primary and the secondary mirrors are close to the simulation and the test data, and most of the detector temperature falls within the range of 5.9—15.8 ℃, which is better than the simulation and the test data, further demonstrating the effectiveness of the design method.

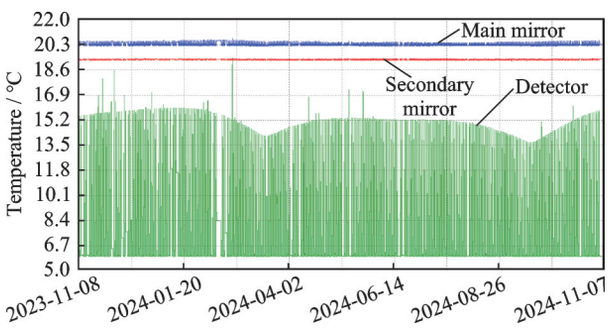

Fig.13 Temperature curves in orbit

3 Conclusions

In order to solve the problem that camera in GEO is susceptible to "Sun transit", a two-layer thermal design method is proposed. By establishing thermal and motion relationships between the avoidance angle and duration ,the results of avoidance angle are obtained.

(1) The avoidance angle obtained by this method is 36.8°, which is reduced by 9.7° compared to traditional methods. This results in a reduction of approximately 10% in both the heat dissipation surface area and the low-temperature compensation power. The results of simulation analysis, thermal balance tests, and in-orbit applications all strongly support the effectiveness of this method.The effectiveness of this method is supported strongly by results of simulation analysis, thermal balance test and in-orbit application.

(2) This method can be applied to more camera design scenarios with sun avoidance requirements. In engineering practice, after determining the

avoidance angle, one should specifically calculate the changes in the heat dissipation surface area and low-temperature compensation power resulting from the implementation of avoidance measures, thereby achieving a complete closed-loop design process.

References

[1] LI Guo, KONG Xianghao. Overview and development trends of high-resolution optical imaging satellite at geostationary orbit[J]. Spacecraft Recovery & Remote Sensing, 2018, 39(4): 55-63. (in Chinese)

[2] WANG Changqing, XIAO Zuolin, ZHANG Qian. Advantage competition of air and space in artificial intelligence era[J]. Transactions of Nanjing University of Aeronautics and Astronautics, 2020, 37(4): 501-507.

[3] LIU Gang, YU Miao. Status and development trends of high-resolution geostationary optical imaging satellite[J]. Flight Control & Detection, 2020, 3(5): 21-27. (in Chinese)

[4] GUO Chongling, CHEN Jiayi, CHEN Chuanzhi, et al. Review on critical technologies for truss structure of large aperture space optical telescope[J]. Journal of Nanjing University of Aeronautics & Astronautics, 2024, 56(1): 31-43. (in Chinese)

[5] TAO Jiasheng, SUN Zhiguo, SUN Yyinghua, et al. Exploration of high resolution optical remote sensing of the geostationary orbit[J]. Opto-Electronic Engineering, 2012, 39 (6): 1-6. (in Chinese)

[6] ZHANG Xuejun, FAN Yanchao, BAO He, et al. Applications and development of ultra large aperture space optical remote sensors[J]. Optics and Precision Engineering, 2016, 24(11): 2613-2626. (in Chinese)

[7] LI Guo, KONG Xianghao, LIU Fengjing, et al. GF-4 satellite remote sensing technology innovation[J]. Spacecraft Recovery & Remote Sensing, 2016, 37 (4): 7-15. (in Chinese)

[8] MA Wenpo, LIAN Minlong. Technical characteristics of the staring camera on board GF-4 satellite[J]. Spacecraft Recovery & Remote Sensing, 2016, 37 (4): 26-31. (in Chinese)

[9] LI Qing, LIU Aifang, WANG Yongmei, et al. Research on development and ability of American space offensive and defensive system[J]. Spacecraft Engineering, 2018, 27(3): 95-103. (in Chinese)

[10] DU Xiaoping, LI Zhi, WANG Yang. Research on the building of US space situational awareness capability[J]. Journal of Equipment Academy, 2017, 28(3): 67-74. (in Chinese)

[11] HE Xingwei, FENG Xiaohu, HAN Qi, et al. Advances of the geostationary meteorological satellite in the world: A review[J]. Advances in Meteorological Science and Technology, 2020, 10(1): 22-29, 41. (in Chinese)

[12] RUDDICK K, NEUKERMANS G, VANHELLEMONT Q, et al. Challenges and opportunities for geostationary ocean colour remote sensing of regional seas: A review of recent results[J]. Remote Sensing of Environment, 2014, 146: 63-76.

[13] RYU J, CHOI J K. Observation on the suspended sediment concentrations in the coastal area using geostationary ocean color imager (GOCI)[C]//Proceedings of the 5th EARSeL Workshop on Remote Sensing of the Coastal Zone. Prague, Czech Republic: EARSeL, 2011: 89-93.

[14] WU Yuhua, CHEN Liheng, LI Hang, et al. Computation of external heat fluxes on space camera with attitude change in geostationary orbit[J]. Infrared and Laser Engineering, 2019, 48(6): 284-292. (in Chinese)

[15] YU Feng, XU Nana, ZHAO Yu, et al. Thermal design and test for space camera on GF-4 satellite[J]. Spacecraft Recovery & Remote Sensing, 2016, 37 (4): 72-79. (in Chinese)

[16] YU Feng, XU Nana, ZHAO Zhenming. On-orbit temperature analysis and thermal design optimization for camera on GF-4 satellite[J]. Journal of Beijing University of Aerinautics and Astronautics, 2021, 47 (1): 177-186. (in Chinese)

[17] ZHAO Zhenming, WANG Bing, GAO Juan. Preliminary research on the thermal design methods of the geosynchronous orbit staring camera[J]. Spacecraft Recovery & Remote Sensing, 2010, 31(3): 34-40. (in Chinese)

[18] XU Nana, YU Feng, FENG Yanguang. Investigation of space heat flux simulation method for remote sensor in geostationary orbit[J]. Spacecraft Recovery & Remote Sensing, 2017, 38(6): 65-73. (in Chinese)

[19] ZHAO Zhenming, LU Pan, SONG Xinyang. Thermal design and test for high resolution space camera on GF-2 satellite[J]. Spacecraft Recovery & Remote Sensing, 2015, 36(4): 34-40. (in Chinese)

[20] SONG Xinyang, GAO Juan, ZHAO Zhenming, et al. Application of indirect thermal control technology for constant temperature control of HR optical remote sensor[J]. Spacecraft Recovery & Remote Sensing, 2015, 36(2): 46-52. (in Chinese)

[21] PENG Zhou, LI Zhensong, QIAO Guodong, et al. Sunlight avoidance design for camera of geostationary orbit remote sensing satellite[J]. Chinese Space Science and Technology, 2045, 35(2): 57-62, 76. (in

Chinese)
[22] LIU Yunhe, LIU Fengjing, YU Longjiang. Sunlight invation avoidance method of GEO optical remote sensing satellite[J]. Spacecraft Engineering, 2014, 23(6): 24-29. (in Chinese)
[23] ZHAO Xin. Analysis of equivalent thermal properties of MLI[J]. Spacecraft Engineering, 2008, 17(4): 51-55. (in Chinese)
[24] ZHANG Yang, ZHAO Jianfeng, HAN Chongwei, et al. Thermal performance equation of multilayer insulator for spacecraft[J]. Chinese Space Science and Technology, 2021, 41(2): 63-70. (in Chinese)
[25] YANG Shiming, TAO Wenquan. Heat transfer [M].4th ed. Beijing, China: Higher Education Press, 2006: 398-402. (in Chinese)
[26] GILMORE D G. Satellite thermal control handbook [M].2nd ed. EI Segundo, USA: The Aerospace Corporation Press,1994.
[27] LEI Zhibo, CAO Jianguang, DONG Lining, et al. Application of high thermal conductivity materials for spacecraft thermal management[J]. Materials Development in China, 2018, 37(12): 1039-1047. (in Chinese)
[28] ZHANG Jianke. Experiment and research for test methods of thermal conductivity of carbon fiber composites at low temperature[J]. Cryogenics, 2010(4): 58-61. (in Chinese)
[29] MIN Guirong. Satellite thermal control technology [M]. Beijing, China: Astronautic Press, 1991. (in Chinese)
[30] HOU Bin. Research progress on thermal control coatings for spacecraft[J]. Modern Radar, 2021, 43(1): 86-90. (in Chinese)

Acknowledgment The work was supported by the National Key Research and Development Program of China (No.2021YFC2202102).

Author

The first/corresponding author Mr. **LIAN Xinhao** received his B.S. degree in chemical machinery from Xi'an Jiaotong University, Shaanxi, China, in 1998 and M.S. degree in aircraft design from Northwestern Polytechnical University, Shaanxi, China, in 2012. In 1998, he joined Beijing Institute of Space Mechanics &Electricity and engaged in research on thermal control technology of space cameras.

Author contributions Mr. **LIAN Xinhao** designed the study, conducted the thermal analysis, interpreted the results and wrote the manuscript. Dr. **XIA Chenhui** conducted the experiments and processed the thermal balance data. Mr. **GAO Chao** designed the experimental device and provided pictures of the camera thermal balance test in progress. All authors commented on the manuscript draft and approved the submission.

Competing interests The authors declare no competing interests.

(Production Editor: ZHANG Bei)

地球静止轨道大口径反射式相机"日凌"耐受能力提升的热控设计方法

连新昊，夏晨晖，高 超
(北京空间机电研究所,北京 100094,中国)

摘要:地球静止轨道大口径反射式相机易受到"日凌"影响导致温度较大波动。针对已有的采用相机遮光罩施加热控措施抑制"日凌"方法的不足和仅通过几何关系确定的太阳光规避角度过大的问题,提出在相机次镜位置增加多层热防护的热控设计方法,力图优化规避角度,提升相机"日凌"耐受能力。建立了规避角度和规避时长之间的热量平衡与运动关系,据此计算了采用多层热防护设计后的最小太阳规避角度,与由几何关系确定的规避角度进行了对比,得出了该方法能够有效提升相机"日凌"耐受能力的结论。提出采用南北耦合散热面设计加低温补偿的内热源散热方案,将两种规避角度的计算结果代入散热面积和低温补偿功率的计算中,在完成散热方案的闭环的同时,从散热面积和低温补偿功率需求角度对比说明了采用多层热防护设计方法的优越性。对比分析了仿真分析、热平衡试验和在轨飞行温度数据,进一步验证了该方法的有效性。

关键词:地球静止轨道;日凌;阳光规避;热控设计;热防护